Supplemental Material

Doubly Transient Chaos: Generic Form of Chaos in Autonomous Dissipative Systems

Adilson E. Motter, Márton Gruiz, György Károlyi, and Tamás Tél

Energy Dissipation Rate and Finite-Time Lyapunov Exponent

Figure S1 summarizes statistical analyses of the average rate of energy dissipation and average finite-time Lyapunov exponent for the undriven dissipative magnetic pendulum.

Driven Dissipative Magnetic Pendulum

It is instructive to compare the autonomous magnetic pendulum with a weakly driven one, which, as we show, does not exhibit super-exponential settling rates. We add time-dependence by moving the three magnets up and down sinusoidally, thus varying the vertical distance as $d = d_0 + d_1 \sin(\Omega t)$, which has the effect of not letting the trajectories rest in their final state. We use $d_0 = 0.3$, $d_1 = 0.1$, and $\Omega = 0.4$, which correspond to the same mean distance as before, a perturbation that leads to a small asymptotic kinetic energy, and a driving frequency smaller than the natural frequency. Under these conditions, long-time motion converges to a persistent swinging of the pendulum in a vertical plane that, by symmetry, passes through the origin and one of the magnets.

Therefore, the system now exhibits three periodic attractors symmetrically disposed, each close to a stable fixed point of the undriven pendulum—see Fig. S2(a) for the $(x, \dot{x})$ projection of one of them. As shown in Fig. S2(b)-(e), the corresponding basins of attraction are at first glance very similar to those of the undriven case (cf. Fig. 1, main text) in that they also consist of interwoven regular and complicated patterns. At this level, the undriven and driven systems seem largely indistinguishable. Moreover, as shown in Fig. S3, at large scales the settling time function of the undriven system seems as complex as that of the driven one.

At very small scales, however, the distribution of diverging peaks of the settling time becomes increasingly sparse for the undriven system [Fig. S3(d)], while systematic changes are far less pronounced for the driven case [Fig. S3(h)]. The change over scales observed in the settling time of the undriven system is directly related to the slim fractal structure of the basin boundaries and is a reflex of the exponentially increasing settling rate caused by energy dissipation. Because we chose to drive the system only weakly to facilitate comparison, the driven system shows systematic changes at large scales, but only until the excess energy is dissipated.

It follows from the corresponding time-dependent free energy function that the settling rate for the driven pendulum tends to a constant rather than an exponentially growing

function (Fig. S4). Again, the scale-dependence observed for small settling times is due to the system being only weakly driven. Thus, the properties of the driven pendulum are similar to those of other such driven dissipative systems previously considered in the literature. On the other hand, the undriven pendulum considered in the main text has fundamentally different properties.
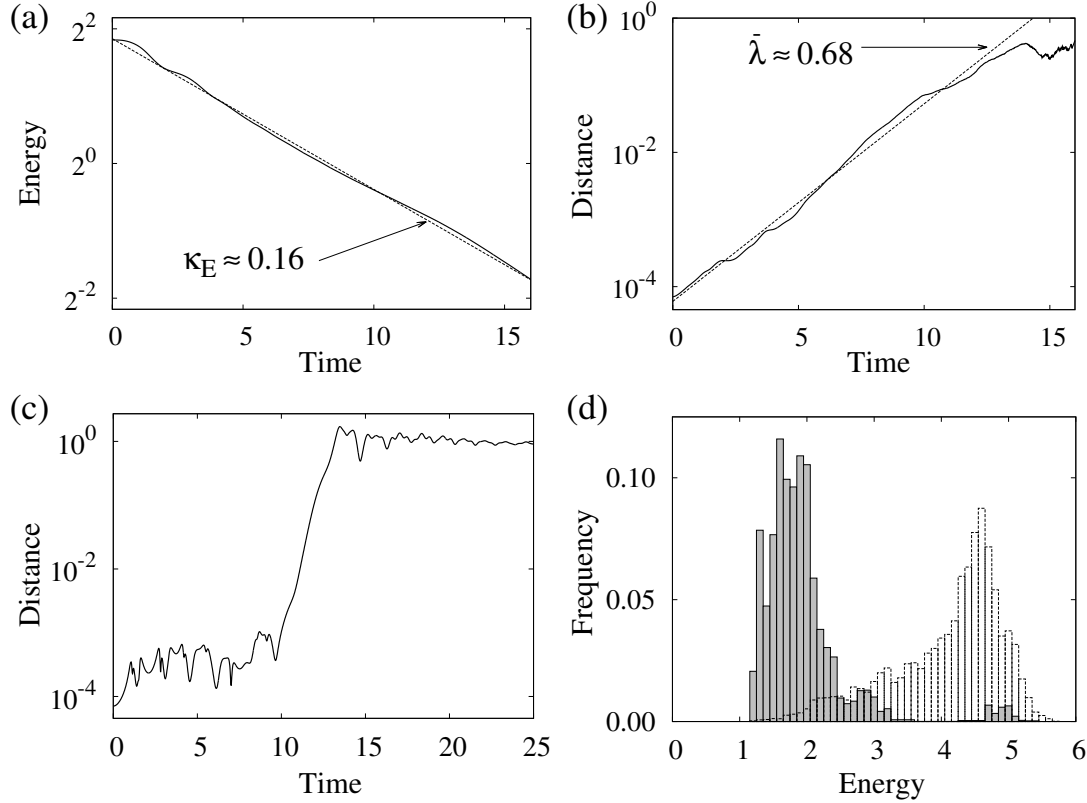

FIG. S1. (a) Average rate of energy dissipation and (b) average finite-time Lyapunov exponent for the autonomous magnetic pendulum. Both quantities were estimated from 20,000 randomly selected initially close pairs of trajectories ($\frac{1}{\sqrt{2}}10^{-4}$ apart) belonging to different basins, sampled with zero initial velocity from the region shown in Fig. 1(b) (main text). (c) Time evolution of the distance between one such pair, showing the period of exponential separation. (d) Distribution of the average energy of the trajectories during the exponential-separation phase. The background histogram shows the initial energy distribution. In (a), the average dissipation rate is close to the damping coefficient α, and for long enough times (not shown) we indeed find $\kappa_E \to \alpha$, as expected for 2D pendulum oscillations around a stable equilibrium. In (b), the time and Lyapunov exponent itself are measured over the period of exponential separation.
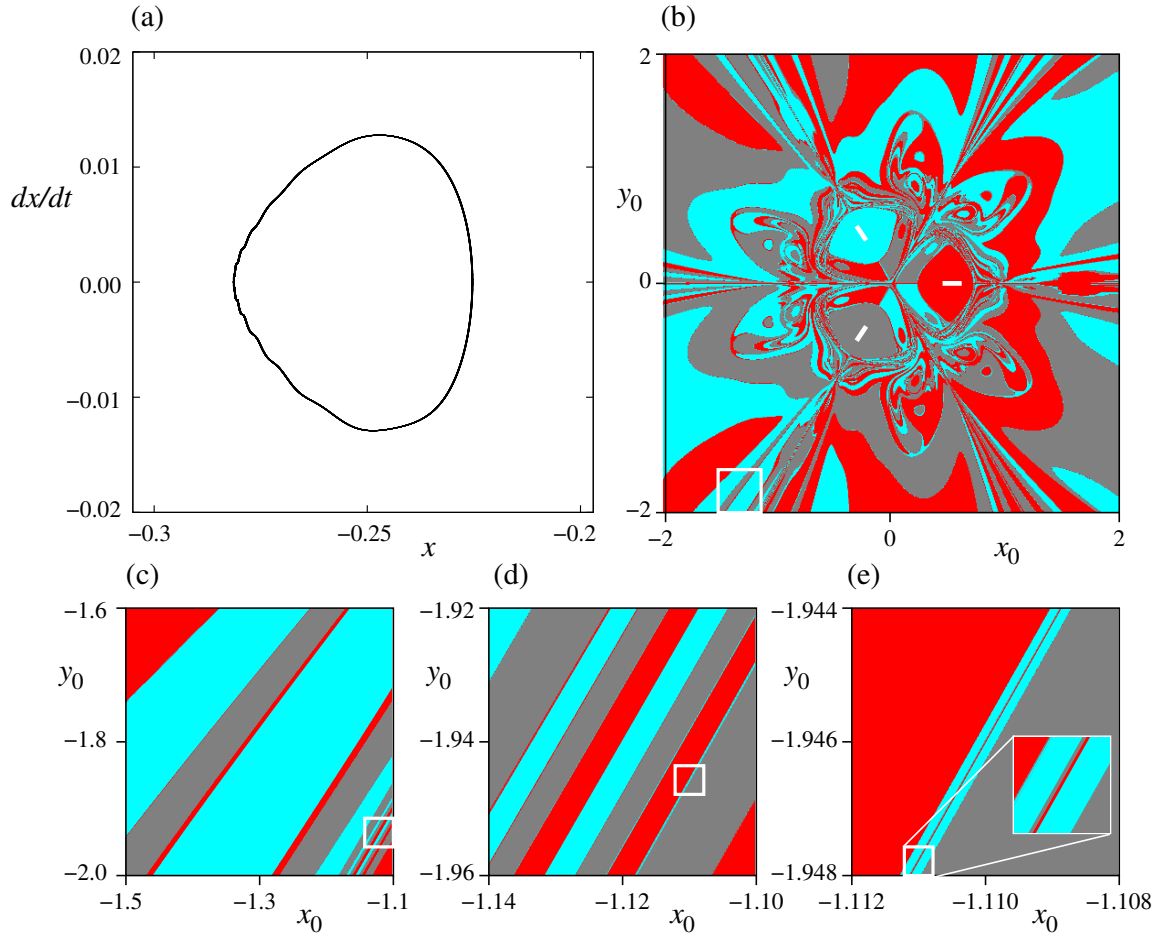
FIG. S2. Phase space of the driven magnetic pendulum. (a) Zoomed-in portrait of one of the three periodic attractors of the system in the $(x, \dot{x})$ projection of the space. (b) Color-coded attraction basins of the three periodic attractors (line segments) for trajectories initiated with zero velocity, as in Fig. 1(b) (main text). (c)-(e) Successive magnifications of the attraction basins.
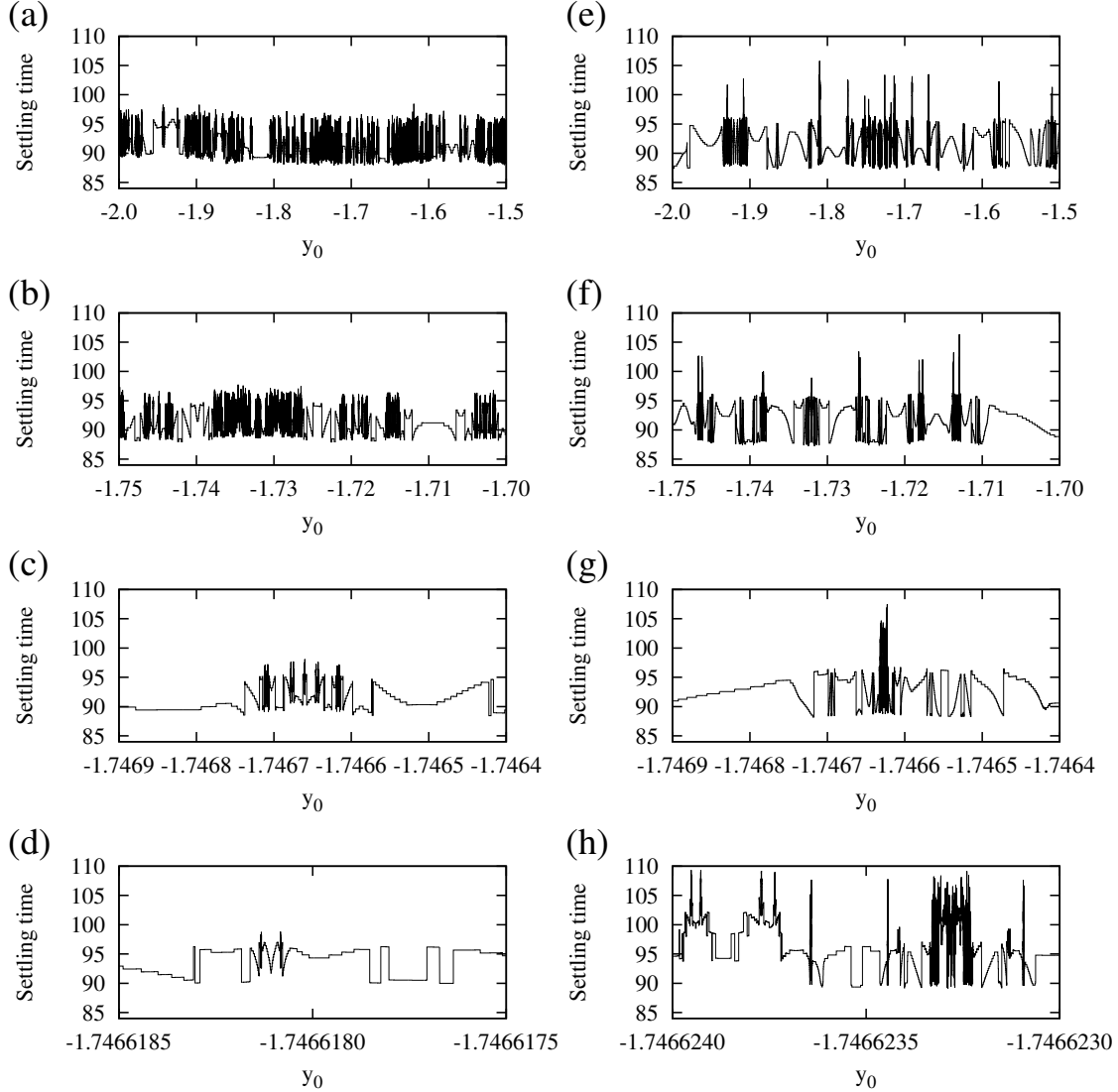
FIG. S3. Settling time functions for the (a)-(d) autonomous and (e)-(h) driven magnetic pendula. The panels show successive magnifications for trajectories initiated with zero velocity on the line $x = -1$ to reach a phase space distance 10^{-4} from an attractor. Over orders of magnitude, the settling time of the autonomous system appears at least as complex as that of the driven system. Only at very small scales it becomes clear that the set of diverging settling times become increasingly sparse in the undriven case, as illustrated in panel (d), while the driven system approaches an approximately self-similar structure at small scales. (The nearly stepwise form of the settling time apparent in the bottom panels is an actual property of the systems rather than an artifact of the resolution.)
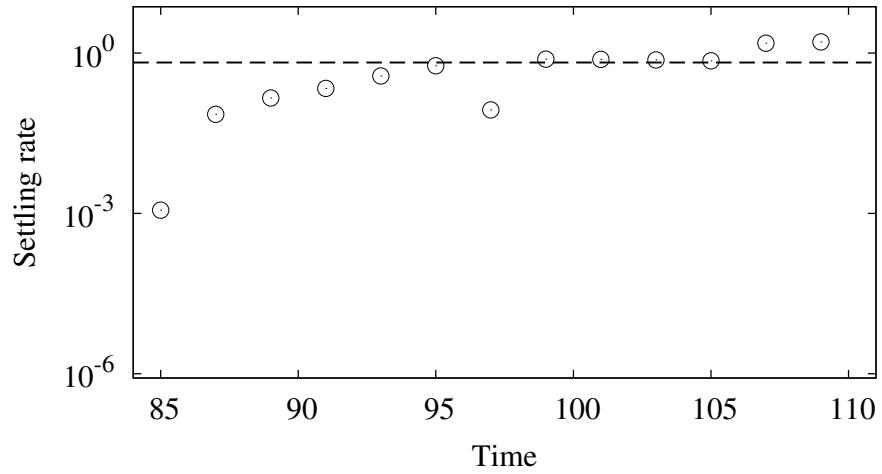
FIG. S4. Time dependence of the settling rate for the driven magnetic pendulum. The trajectories are initiated with zero velocity on the line $x = -1$ and are considered settled once their phase-space distance to an attractor becomes smaller than 10^{-4}. The circles represent the numerical results, while the dashed line is a guide to the eye. As for other driven dissipative systems, the settling rate in this case approaches a constant rather than an exponentially growing function.